Effects of hole doping on magnetic and lattice excitations in $Sr_2Ir_{1-x}Ru_xO_4$ ($x = 0$–0.2)

A. Glamazda, W.-J. Lee, and K.-Y. Choi*
Department of Physics, Chung-Ang University, 221 Huksuk-Dong, Seoul 156-756, Republic of Korea

P. Lemmens
Institute for Condensed Matter Physics, TU Braunschweig, D-38106 Braunschweig, Germany

H. Y. Choi, N. Lee, and Y. J. Choi
Department of Physics and IPAP, Yonsei University, Seoul 120-749, Republic of Korea

(Received 3 November 2013; revised manuscript received 26 January 2014; published 10 March 2014)

Raman scattering is employed to explore the effects of hole doping in single crystals of $Sr_2Ir_{1-x}Ru_xO_4$ ($x = 0$, 0.01, 0.03, 0.05, 0.1, and 0.2). Introducing a few percentages of holes has a strong impact on magnetic excitations and lattice dynamics. With increasing x the well structured two-magnon continuum turns into diffusive magnetic scattering. Furthermore one- and two-phonon scatterings are rapidly suppressed. Remarkably, the two Ir(Ru)-O-Ir(Ru) bond angle modes with different Ir(Ru)O_6 octahedral rotations coexist and compete upon hole doping. This is ascribed to the difference of electronic properties between Ir^{4+} and Ru^{4+} ions. The doping and temperature dependence of the bond angle modes suggests that an electronically phase separated state develops upon Ru doping.

DOI: 10.1103/PhysRevB.89.104406 PACS number(s): 78.30.Am, 75.30.Kz, 63.20.Dj

I. INTRODUCTION

In recent years, there has been an upsurge of research interest in $5d$ transition metal oxides, in which spin-orbit coupling (SOC) is comparable to on-site Coulomb repulsion (U) and one-electron bandwidth (W). Strong SOC entangles spin and orbital spaces and thus leads to the formation of SO coupled narrow bands and unconventional spin and orbital magnetic moments. This is responsible for novel electronic and magnetic properties of layered iridium oxides, such as Sr_2IrO_4, $Sr_3Ir_2O_7$, and A_2IrO_3 (A = Na, Li) [1–6].

In the present study, we focus on the Mott insulator Sr_2IrO_4, which crystallizes in a distorted tetragonal structure (space group $I4_1/acd$). The Ir^{4+} ions on a square lattice are connected by corner-sharing IrO_6 octahedra. The IrO_6 octahedra are elongated along the c axis and alternately rotated with respect to the c axis by about 11° [7]. The compound undergoes antiferromagnetic ordering at $T_N = 240$ K with large ferromagnetic moments [$0.208(3)\mu_B$/Ir site] within the basal plane accompanying in-plane rotations of the IrO_6 octahedra [8,9,10]. A recent x-ray resonant magnetic scattering study has refined the magnetic structure of Sr_2IrO_4 and unveiled that the antiferromagnetic component lies along the a axis while a net b-axis ferromagnetic moment occurs due to a canting of the magnetic moments by $12.2(8)^\circ$ from the a axis [11,12]. The notable thing is that the canting of the Ir magnetic moments follows the rotation of the oxygen octahedra. A strong connection between the crystal and magnetic structure is further manifested in a metamagnetic transition at about 110 K which results from modulations of the Ir-O-Ir bond angle [13].

The low-lying t_{2g} band consists of fully filled $J_{\text{eff}} = 3/2$ bands and a narrow, half-filled $J_{\text{eff}} = 1/2$ band near the Fermi energy [5,14]. The narrow $J_{\text{eff}} = 1/2$ band splits into Mott-Hubbard bands in the presence of a moderate on-site Coulomb repulsion [15]. The SO induced J_{eff} level scheme has been supported by optical absorption and resonant inelastic x-ray scattering (RIXS) measurements [4,14,16–18]. In a recent RIXS study the observation of strongly dispersing SO excitons in the energy range of 0.4–0.8 eV has been reported. The gradual renormalization of the optical absorption with increasing temperature indicates a reduction and filling of the Mott-Hubbard gap with temperature. Raman scattering evidenced a crossover from coherent to incoherent scattering, which is related to excitonlike orbital excitations that decay into magnon excitations [19].

Very recently, the Mott mechanism has been challenged. X-ray absorption spectroscopy, time-resolved optical studies, and a scanning tunneling microscopy/spectroscopy support a Slater-type scenario in which the insulating gap is opened by magnetic ordering [20–23]. Given this result, Sr_2IrO_4 may be close to the boundary of a Mott insulator, that is, $U \sim W$. Epitaxial strain studies in thin films reveal that both electronic bandwidth and electronic correlations changes in an intriguing manner under lattice strain [24].

In the vicinity of a SO-induced Mott insulator, a variety of competing electronic phases have been predicted [25,26]. An effective way to tune electronic parameters, i.e., U and W, is chemical doping. Experimental investigations of the hole-doped $Sr_2Ir_{1-x}Ru_xO_4$ have been conducted on polycrystalline samples and thin films [27–30]. However, the unavailability of single crystals makes it difficult to fully characterize their physical properties. Hence, single-crystal studies are called for to figure out the evolution of magnetic, electronic, and structural properties as a function of doping.

In this paper, we have employed Raman spectroscopy to address the aforementioned issues in single crystals of $Sr_2Ir_{1-x}Ru_xO_4$ ($x = 0$, 0.01, 0.03, 0.05, 0.1, and 0.2). The previous Raman study of the undoped Sr_2IrO_4 single crystals

*kchoi@cau.ac.kr

has observed an interesting interplay of electronic and lattice modes as functions of temperature and excitation wavelength [19]. We observe that hole doping has a similar drastic effect on electronic and magnetic properties as temperature does. The major finding is the coexistence of the two Ir(Ru)-O-Ir(Ru) bond angle modes with different Ir(Ru)O_6 octahedral rotations in the studied doping range. This demonstrates the formation of an electronically phase separated state upon a hole doping.

II. EXPERIMENTAL DETAILS

Single crystals of $Sr_2Ir_{1-x}Ru_xO_4$ ($x = 0$, 0.01, 0.03, 0.05, 0.1, and 0.2) were grown by the flux method [4]. The low hole-doped samples exhibit semiconducting behavior. Upon 20% Ru doping, the cell volume changes less than by 0.5% and the crystal symmetry remains unaltered [27].

For Raman scattering measurements, single crystals with dimensions of $1 \times 0.5 \times 0.2$ mm^3 were used. Raman spectroscopic studies were carried out in quasi-backscattering geometry with the excitation line $\lambda = 532$ nm and laser power $P = 10$ mW of a solid state laser. Temperature was varied between 5 and 300 K by using a closed-cycle cryostat. The spectra were collected by a DILOR-XY triple spectrometer and a micro-Raman setup (Horiba Labram) equipped with a nitrogen-cooled charge-coupled device detector.

III. RESULTS AND DISCUSSION

A. Doping dependence of low-energy phonon modes

In Fig. 1 we compare Raman spectra of $Sr_2Ir_{1-x}Ru_xO_4$ ($x = 0$, 0.03, 0.1, and 0.2) measured at $T = 287$ and 7 K in (xu) polarization, i.e., without a polarization analyzer. This is intended to maximize the scattering intensity. We note that the (xu) polarization spectra contain the same information about phonons as the (xx) polarization ones. For the undoped sample,

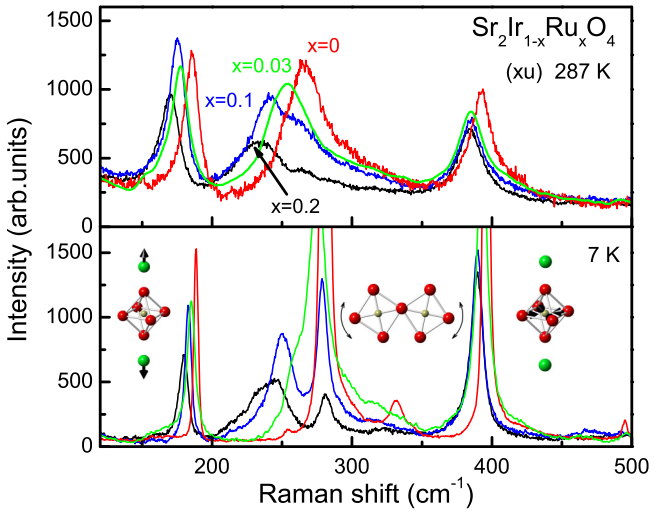

FIG. 1. (Color online) Raman spectra of $Sr_2Ir_{1-x}Ru_xO_4$ ($x = 0$, 0.03, 0.1, and 0.2) at $T = 7$ K (lower panel) and 287 K (upper panel) in (xu) polarization. The insets depict the eigenvectors of the 188, 278, and 392 cm^{-1} modes. The relative amplitude of the vibrations is given by the arrows. The green balls stand for the Sr ions, the grey ones for Ir(Ru) ions, and the red ones for the oxygen ions

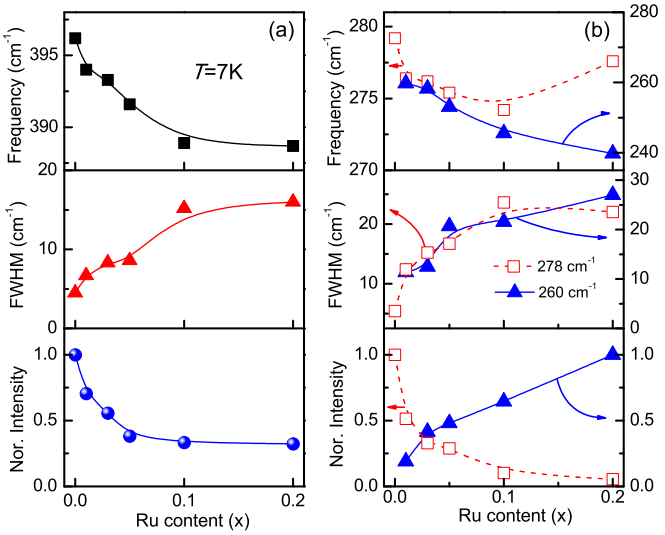

FIG. 2. (Color online) Frequencies, full widths at half maximum, and integrated intensities of the phonons at 392 and 278 cm^{-1} as a function of Ru doping.

our results are fully consistent with the previous Raman data on undoped single crystals. We refer to Ref. [19]. for the complete assignments of the phonon modes. The comparison shows, furthermore, that there are no substantial Ru doping effects on the high-frequency phonon modes. This is different for the low-energy phonon modes, which we will focus on in the following.

At room temperature we observe three main peaks at 188, 278, and 392 cm^{-1} in the intermediate frequency range. As depicted in the inset of Fig. 1, the 188 cm^{-1} A_{1g} mode corresponds to stretching vibrations of the Sr atoms with respective to IrO_6 along the c axis. The 278 cm^{-1} mode involves bending motions of the Ir-O-Ir bonds; more specifically, rotations of the corner-sharing octahedra about the center oxygens within the ab plane. The 392 cm^{-1} A_{1g} mode is assigned to the displacements of the in-plane oxygen atoms of the octahedron relative to each other [31].

With decreasing temperature three phonons increase in intensity and decrease in linewidth. As x increases, the phonon modes undergo a substantial change in frequency and intensity. To quantify the phonon parameters, the Raman spectra are fitted to a sum of Lorentzian profiles. The resulting parameters are summarized in Fig. 2 as a function of x.

In the studied doping range of $x = 0$–0.2 we observe the intriguing variations of the phonon parameters with x. Considering that the lattice parameters follow the Vegard's law with a linear shrinkage [27], this is due to the electronic and local structural changes induced by the Ru doping. In Fig. 2(a) we plot the doping dependence of the 392 cm^{-1} mode at $T = 7$ K. The 188 cm^{-1} mode shows essentially the same behavior (not shown here). With increasing x, the 392 cm^{-1} mode undergoes a large softening by 8 cm^{-1}, a line broadening by about three times, and an exponential-like reduction of the scattering intensity. Noticeably, the drastic changes occur in the low-doing concentrations of $x = 0$–0.05. This points to the strong impact of the small Ru doping on electronic and local structural properties.

The most salient feature is observed at the 278 cm^{-1} mode. With increasing x, the 278 cm^{-1} mode is drastically suppressed while the new mode at 260 cm^{-1} develops in the lower-frequency side of the 278 cm^{-1} mode (see the lower panel of Fig. 1). Here we will not discuss the higher-frequency feature due to its weak intensity. As plotted in Fig. 2(b), the 260 cm^{-1} mode (blue full triangles) softens by 20 cm^{-1} in a monotonic manner. The 278 cm^{-1} principal mode (red open squares) shows a similar softening up to $x = 0.1$ while undergoing a large increase of its frequency at $x = 0.2$. As to the linewidth, both modes exhibit a large broadening in the doping range of $x = 0$–0.05 and then almost saturation for $x \geqslant 0.1$. The integrated intensity of the 278 cm^{-1} mode decreases rapidly with increasing x. In contrast, the 260 cm^{-1} mode shows a quasi-linear increase of the intensity. This contrasting behavior indicates the occurrence of the two competing states upon Ru doping. The coexistence of the competing state implies that the doping induces an electronically phase separated state [27].

We remind that the 278 cm^{-1} mode directly probes a modulation of the Ir-O-Ir bond angle and shows a large temperature dependence for the undoped sample [18,19]. This is correlated with the reduction in the Ir-O-Ir bond angle from 157.28° at room temperature to 156.56° at $T = 10$ K [7,8]. Also, the Ir(Ru)-O-Ir(Ru) bond angle increases from 158° for $x = 0$ to 180° for $x = 1$ [27,32]. Accordingly, the rotation of the IrO_6 octahedra about the c axis is reduced as x increases. For a homogeneous electric state we thus expect a monotonic softening of the 278 cm^{-1} mode with increasing Ru doping. However, we observe the nonmonotonic doping dependence of its frequency [see the open squares in Fig. 2(b)]. Moreover, a tiny amount of Ru doping induces the new mode, suggesting the local inhomogeneity of the Ir(Ru)O_6 octahedral rotation pattern. That means that at low Ru dopings holes remain largely localized within an electronically phase separated state. This may be because a Mott gap blocks a charge transfer from Ru^{4+} to Ir^{4+} ions [10].

B. Doping dependence of magnetic excitations

Figure 3 displays Raman spectra in (xx) polarization of $Sr_2Ir_{1-x}Ru_xO_4$ ($x = 0$, 0.03, 0.1, and 0.2) at 7 K taken in a wide frequency range of 180–2700 cm^{-1}. We observe an asymmetric, broad continuum centered at 1750 cm^{-1}, which is of magnetic origin. The previous Raman scattering study with resonant excitation reveals the unconventional features of these excitations [19]: (i) a drastic suppression of the magnetic scattering intensity for $T > T_N$ which is uncommon for two-magnon scattering in insulating materials, (ii) a high-energy tail and asymmetric linewidth, and (iii) the crossover of two-magnon to incoherent, fluorescent-like scattering with higher excitation energy. These effects are discussed in terms of intertwined spin and charge excitations as well as the existence of an exciton regime.

Upon introducing holes, the two-magnon continuum is substantially suppressed in intensity and shifts to lower energies. The doping effects on the isospin $J_{\rm eff} = 1/2$ iridates are much more salient than on the $s = 1/2$ high-T_C cuprates [33]. In cuprates, A-site doping leads to the filling of d bands on the B sites by donating its valence electrons. Introduced holes become mobile and destroy long-range

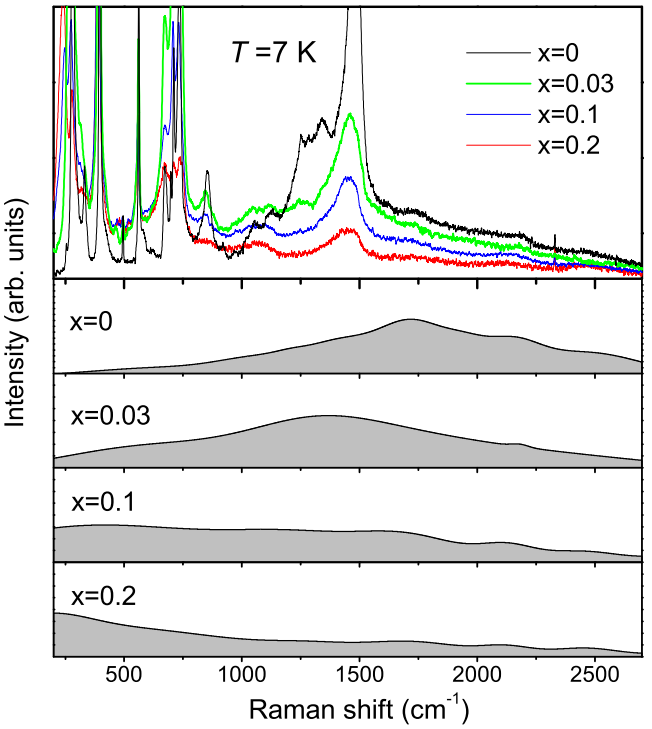

FIG. 3. (Color online) (Upper panel) Raman spectra of $Sr_2Ir_{1-x}Ru_xO_4$ ($x = 0$, 0.03, 0.1, and 0.2) measured in a wide-frequency range at $T = 7$ K. (Lower panels) Doping dependence of the magnetic continua obtained by subtracting the phonon peaks.

antiferromagnetic ordering to gain kinetic energy of the holes. However, short-range correlations persist for doping well above the optimal doping regime. Thus, the two-magnon continuum retains its characteristic maximum related to high-energy spin correlations at the zone boundary. For the case of $Sr_2Ir_{1-x}Ru_xO_4$, B-site doping adds nominally holes onto the IrO_2 planes while introducing impurities into the $J_{\rm eff} = 1/2$ magnetic background. As a result, the Ru doping causes a multifaceted perturbation to magnetic excitations. On the one hand, the introduction of holes increases the bandwidth, reduces spin-orbit coupling, and alters the density of electronic states. On the other hand, the occupation of two different ions at the B-site leads to a formation of an electronically inhomogeneous phase. Since charge excitations are involved in the two-magnon excitation process of the iridate, spin excitations will be damped rapidly upon Ru doping.

In addition to the magnetic excitations, the one- and two-phonon scattering show substantial doping effects as well. In Fig. 4 we compare the doping dependence of the normalized integrated intensities of the one-phonon peak at 730 cm^{-1}, the two-phonon peak at 1470 cm^{-1}, the ratio of the two- to the one-phonon mode, and the two-magnon continuum. With increasing x, they exhibit a monotonic, substantial decrease. This suggests that both magnetic and lattice excitations are strongly affected in the presence of a small amount of holes.

We note that in resonant Raman scattering, the one-phonon intensity is given by $I_1 \sim (\omega - \omega_{fi})^{-4}$ while the second-order scattering by $I_2 \sim (\omega - \omega_{fi})^{-6}$ [34]. Here ω_{fi} is the interband energy. The intensity ratio $I_2/I_1 \sim (\omega - \omega_{fi})^{-2}$ varies with ω_{fi}. Therefore, the x dependence of I_2/I_1 confirms that

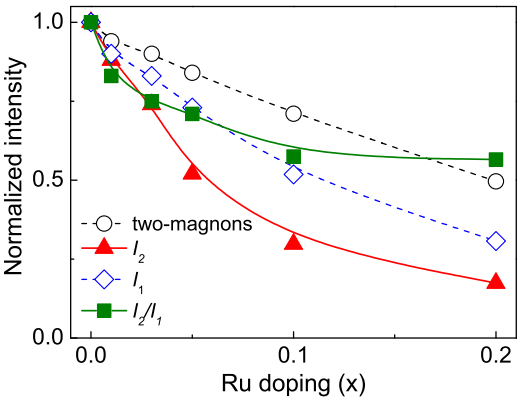

FIG. 4. (Color online) Normalized integrated intensities of two-magnon scattering, one-phonon scattering at 730 cm^{-1} (I_1), two-phonon scattering at 1470 cm^{-1} (I_2), and the ratio (I_2/I_1) as a function of x.

the pronounced two-phonon scattering is due to a resonant mechanism. This is plausible because the resonance condition is expected to weaken due to the modification of electronic states by the B-site doping. We stress that both the magnetic and higher-order phonon scattering are susceptible to changes of the electronic state. This observation is indicative of strong couplings among electronic, magnetic, and lattice degrees of freedom. This is further supported by the recent angle-resolved photoemission result, which provides evidence for a polaronic ground state [35].

C. Temperature dependence of out-of-plane phonon modes at $x = 0$

In Fig. 5 we compare Raman spectra of the undoped Sr_2IrO_4 with in-plane and with out-of-plane polarization. The low-temperature spectra markedly differ from each other. Both the two-magnon and two-phonon scattering are almost suppressed in (zz) polarization. The anisotropic magnetic and higher-order phonon response demonstrates that their

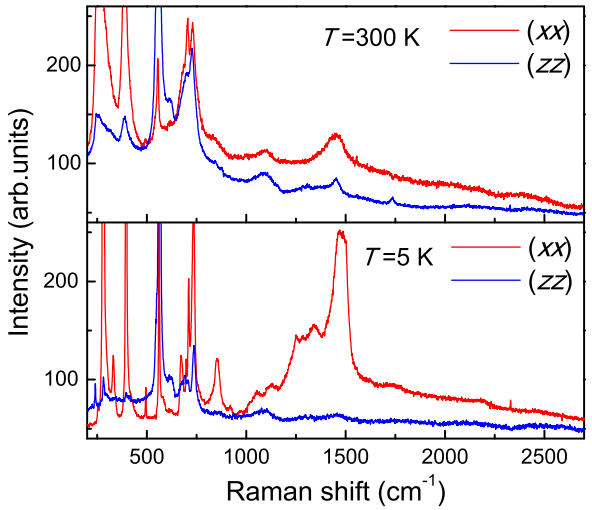

FIG. 5. (Color online) Comparison of the undoped Raman spectra for (xx) and (zz) polarization at $T = 5$ and 300 K.

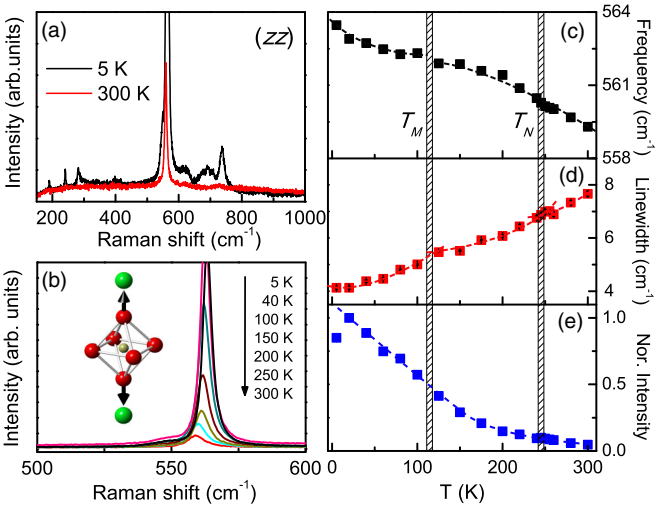

FIG. 6. (Color online) (a) Comparison of Raman spectra at $T = 5$ and 300 K in (zz) polarization. (b) Temperature dependence of the 563 cm^{-1} mode with a sketch of its normal mode displacement. (c)–(e) Temperature dependence of frequency, linewidth, and normalized intensity of the 563 cm^{-1} mode, respectively.

origin is rooted in highly anisotropic, layered electronic states. The absence of a magnetic signal in (zz) polarization for temperatures below T_N is characteristic for the K_2NiFe-type antiferromagnet as reported in $LaSrMnO_4$ [36]. Within the exchange light scattering approximation, the Raman operator is proportional to $\mathcal{R} \propto S_i \cdot S_j$. Thus, magnetic scattering is negligible in interplane polarizations because of weak interplane interactions.

At high temperatures quasielastic scattering becomes pronounced in (zz) polarization so that the (zz) spectrum resembles the (xx) one but with a weaker intensity. The mechanism of a quasielastic response is totally different from that of two-magnon scattering [37]. It is due to diffusive fluctuations of a four-spin time correlation function or fluctuations of the magnetic energy density. The quasielastic response often governs magnetic Raman scatterings in low-dimensional antiferromagnets.

As to phonons, we observe the strong peak at 563 cm^{-1} as shown in Fig. 6(a). This is assigned to the A_{1g} mode, which corresponds to vibrations of apical oxygens along the z axis [see the inset of Fig. 6(b)] [36]. With decreasing temperature down to $T = 5$ K, a dozen weak peaks show up, which are part of the symmetry-allowed $4A_{1g} + 16E_g$ modes for the $I4_1/acd$ crystal symmetry [19,38,39]. Remarkably, the 563 cm^{-1} mode varies strongly with temperature. The phonon parameters are plotted in Figs. 6(c)–6(e). In contrast to the low-energy modes, the 563 cm^{-1} mode shows a moderate frequency shift. However, we cannot reproduce the temperature dependence of frequency and linewidth in terms of an anharmonic phonon model (not shown here). Rather, we identify discernible anomalies at T_N and T_M. In the studied system, a strong magnetoelastic coupling arises due to the fact that the Ir magnetic moments rotate with the IrO_6 octahedra [9,11,12].

The sensitivity of the apical oxygen mode to the metamagnetic transition at T_M indicates that it is caused by modulations

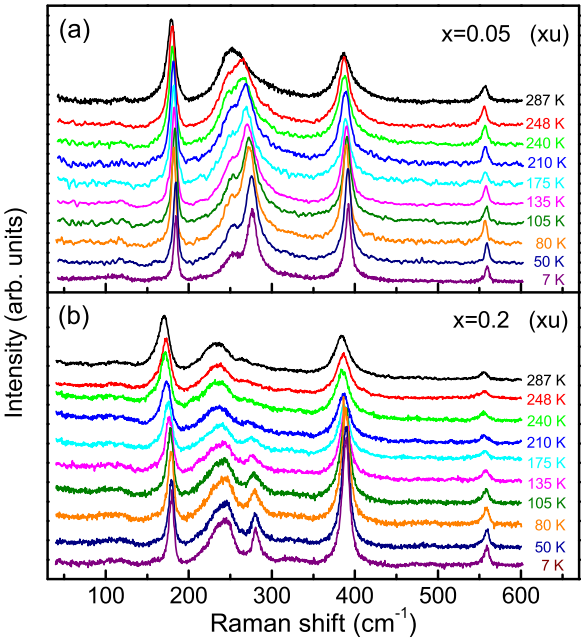

FIG. 7. (Color online) Temperature dependence of Raman spectra of $x = 0.05$ (upper panel) and $x = 0.2$ (lower panel) in the temperature range of $T = 7$–287 K measured in (xu) polarization.

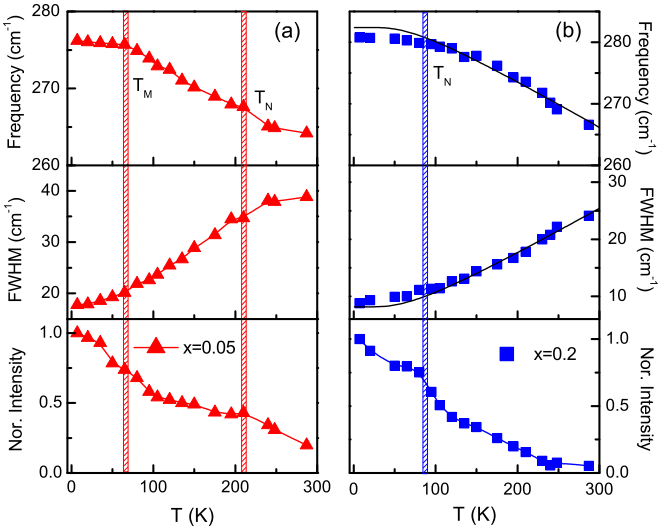

FIG. 8. (Color online) Temperature dependence of the frequency, linewidth, and normalized integrated intensities of the 278 cm^{-1} mode for (a) $x = 0.05$ and (b) $x = 0.2$. The integral intensities are corrected by the Bose-Einstein thermal factor. The solid lines are fits to an anharmonic model.

of the IrO_6 octahedron. This provides additional evidence that magnetism is controlled by structural parameters. This also explains the anomalously large change in intensity for temperatures below T_N. The reduction of the Ir-O-Ir bond angle with lowering temperature is expected to alter electronic density of states. This changes the resonance condition and the polarizability of the wave functions and, thus, finally the phonon intensity as a function of temperature.

D. Temperature dependence of phonon modes at $x = 0.05$ and $x = 0.2$

We now turn to the temperature dependence of the Raman spectra in the doped samples. As presented in Fig. 7, for the $x = 0.05$ and $x = 0.2$ crystals all phonons become intense and sharpen with decreasing temperature. Particularly, the bond angle modes exhibit anomalous temperature dependence. To detail the evolution of phonon parameters, the spectra are fitted to a sum of Lorentzian profiles. In Fig. 8 we summarize the temperature dependence of the frequency, the full width at half maximum, and the normalized intensity of the 278 cm^{-1} mode.

Both compounds show the large softening of the 278 cm^{-1} mode by 14 cm^{-1} (5%). This is related to an increase in the rotation angle of the $Ir(Ru)O_6$ octahedra with decreasing temperature [8,32]. For $x = 0.05$, we are able to identify two anomalies at about $T_N = 210$ K and $T_M = 70$ K. These correspond to the antiferromagnetic and the metamagnetic transitions, respectively. Compared to the undoped sample, they are shifted to lower temperature by 30 K, consistent with a suppression of the magnetic ordering. Upon further increasing doping to $x = 0.2$, the frequency and the linewidth seem to show no apparent anomalies while the intensity exhibits an abrupt increase at about $T_N = 90$ K. We try to describe the temperature dependence of the frequency and linewidth in terms of an anharmonic interaction model. This provides a satisfactory description to the data for temperatures above T_N. There appear small deviations for temperatures below T_N.

To quantify the variation of competing lattice distortions with temperature, we plot the relative intensity of the 278 cm^{-1} to the 254 cm^{-1} mode, $I_{278}/I_{254}(T)$ for $x = 0.05$ and $x = 0.2$ in Fig. 9. For both compounds, with decreasing temperature the relative intensity increases steeply with the distinct anomalies at the magnetic transition temperatures. This means that the 278 cm^{-1} mode undergoes a more drastic change than the 254 cm^{-1} mode (see also Fig. 7). Further, this result suggests that the lattice distortion pertaining to the 278 cm^{-1} mode

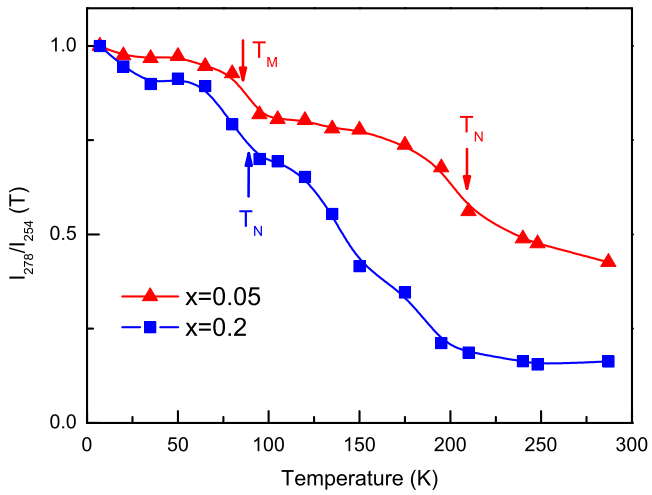

FIG. 9. (Color online) Temperature dependence of the relative intensity of the 278 cm^{-1} to the 254 cm^{-1} mode for $x = 0.05$ and $x = 0.2$. The ratio is normalized by the value at $T = 7$ K.

plays a decisive role in stabilizing the Mott insulating state and thus the magnetic ordering.

IV. CONCLUSION

To summarize, we have presented a Raman scattering study on single crystals of $Sr_2Ir_{1-x}Ru_xO_4$ ($x = 0$–0.2). We adopted hole doping and temperature as experimental parameters. In a previous study Cetin *et al.,* [19] showed a suppression of a magnetic signal at T_N for $x = 0$. Our results support this data and further demonstrate that the introduction of holes rapidly weakens magnetic and lattice excitations. This evidences that magnetic, structural, and electronic properties are closely tied. A small perturbation in one parameter will thus have a ubiquitous influence on all parameter spaces. We expect magneto-dielectric effects due to field-induced modification of the IrO_6 octahedra, which should be examined in future work.

The most prominent observation of the present work is the coexistence of the Ir(Ru)-O-Ir(Ru) bond angle modes with different $Ir(Ru)O_6$ octahedral rotations in the studied doping range. With increasing x the lower-frequency mode becomes stronger than the high-frequency one. The occurrence of two competing lattice distortions implies that $Sr_2Ir_{1-x}Ru_xO_4$ has an inhomogeneous magnetic, structural, and electronic state. This is discussed in terms of the Ru substitution onto Ir^{4+} site, causing an electronic phase segregation because a charge transfer from Ru^{4+} to Ir^{4+} ions is blocked by a Mott gap.

ACKNOWLEDGMENTS

We thank J. S. Hwang for insightful discussions. K.Y.C. acknowledges financial support from Korea NRF Grants (No. 2009-0093817 and No. 2012-046138). This work was supported by NTH (Contacts in Nanosystems), the German-Israeli Foundation (GIF, 1171-189.14/2011), and the German Science Foundation (DFG, SPP 1458 and 1666). The work at Yonsei University was supported by NRF Grants (NRF-2012M2B2A4029730 and NRF-2013R1A1A2058155) and by the BK21 Plus project. N.L. was supported partially by the Yonsei University Research Fund of 2012.

[1] L. J. P. Ament, G. Khaliullin, and J. van den Brink, Phys. Rev. B **84**, 020403(R) (2011).
[2] J. Chaloupka, G. Jackeli, and G. Khaliullin, Phys. Rev. Lett. **105**, 027204 (2010).
[3] B. J. Kim, Hosub Jin, S. J. Moon, J.-Y. Kim, B.-G. Park, C. S. Leem, Jaejun Yu, T. W. Noh, C. Kim, S.-J. Oh, J.-H. Park, V. Durairaj, G. Cao, and E. Rotenberg, Phys. Rev. Lett. **101**, 076402 (2008).
[4] B. J. Kim, H. Ohsumi, T. Komesu, S. Sakai, T. Morita, H. Takagi, and T. Arima, Science **323**, 1329 (2009).
[5] G. Jackeli and G. Khaliullin, Phys. Rev. Lett. **102**, 017205 (2009).
[6] B. H. Kim, G. Khaliullin, and B. I. Min, Phys. Rev. Lett. **109**, 167205 (2012).
[7] Q. Huang, J. L. Soubeyroux, O. Chmaissen, I. Natali Sora, A. Santoro, R. J. Cava, J. J. Krajewski, and W. F. Peck, Jr., J. Solid State Chem. **112**, 355 (1994).
[8] M. K. Crawford, M. A. Subramanian, R. L. Harlow, J. A. Fernandez-Baca, Z. R. Wang, and D. C. Johnston, Phys. Rev. B **49**, 9198 (1994).
[9] F. Ye, S. Chi, B. C. Chakoumakos, J. A. Fernandez-Baca, T. Qi, and G. Cao, Phys. Rev. B **87**, 140406(R) (2013).
[10] C. Dhital, T. Hogan, W. Zhou, X. Chen, Z. Ren, M. Pokharel, Y. Okada, M. Heine, W. Tian, Z. Yamani, C. Opeil, J. S. Helton, J. W. Lynn, Z. Wang, V. Madhavan, and S. D. Wilson, Nat. Commun. **5**, 3377 (2014).
[11] S. Boseggia, R. Springell, H. C. Walker, H. M. Rønnow, Ch. Ruegg, H. Okabe, M. Isobe, R. S. Perry, S. P. Collins, and D. F. McMorrow, Phys. Rev. Lett. **110**, 117207 (2013).
[12] S. Boseggia, H. C. Walker, J. Vale, R. Springell, Z. Feng, R. S. Perry, M. Moretti Sala, H. M. Rønnow, S. P. Collins, and D. F. McMorrow, J. Phys.: Condens. Matter **25**, 422202 (2013).
[13] S. Chikara, O. Korneta, W. P. Crummett, L. E. DeLong, P. Schlottmann, and G. Cao, Phys. Rev. B **80**, 140407(R) (2009).
[14] S. J. Moon, M. W. Kim, K. W. Kim, Y. S. Lee, J.-Y. Kim, J.-H. Park, B. J. Kim, S.-J. Oh, S. Nakatsuji, Y. Maeno, I. Nagai, S. I. Ikeda, G. Cao, and T. W. Noh, Phys. Rev. B **74**, 113104 (2006).
[15] C. Martins, M. Aichhorn, L. Vaugier, and S. Biermann, Phys. Rev. Lett. **107**, 266404 (2011).
[16] K. Ishii, I. Jarrige, M. Yoshida, K. Ikeuchi, J. Mizuki, K. Ohashi, T. Takayama, J. Matsuno, and H. Takagi, Phys. Rev. B **83**, 115121 (2011).
[17] J. Kim, D. Casa, M. H. Upton, T. Gog, Y.-J. Kim, J. F. Mitchell, M. van Veenendaal, M. Daghofer, J. van den Brink, G. Khaliullin, and B. J. Kim, Phys. Rev. Lett. **108**, 177003 (2012).
[18] S. J. Moon, H. Jin, W. S. Choi, J. S. Lee, S. S. A. Seo, J. Yu, G. Cao, T. W. Noh, and Y. S. Lee, Phys. Rev. B **80**, 195110 (2009).
[19] M. F. Cetin, P. Lemmens, V. Gnezdilov, D. Wulferding, D. Menzel, T. Takayama, K. Ohashi, and H. Takagi, Phys. Rev. B **85**, 195148 (2012).
[20] D. Haskel, G. Fabbris, M. Zhernenkov, P. P. Kong, C. Q. Jin, G. Cao, and M. van Veenendaal, Phys. Rev. Lett. **109**, 027204 (2012).
[21] D. Hsieh, F. Mahmood, D. H. Torchinsky, G. Cao, and N. Gedik, Phys. Rev. B **86**, 035128 (2012).
[22] Q. Li, G. Cao, S. Okamoto, J. Yi, W. Lin, B. C. Sales, J. Yan, R. Arita, J. Kunes, A. V. Kozhevnikov, A. G. Eguiluz, M. Imada, Z. Gai, M. Pan, and D. G. Mandrus, Sci. Rep. **3**, 3073 (2013).
[23] R. Arita, J. Kunes, A. V. Kozhevnikov, A. G. Eguiluz, and M. Imada, Phys. Rev. Lett. **108**, 086403 (2012).
[24] J. Nichols, J. Terzic, E. G. Bittle, O. B. Korneta, L. E. De Long, J. W. Brill, G. Cao, and S. S. A. Seo, Appl. Phys. Lett. **102**, 141908 (2013).
[25] D. Pesin and L. Balents, Nat. Phys. **6**, 376 (2010).
[26] F. Wang and T. Senthil, Phys. Rev. Lett. **106**, 136402 (2011).
[27] R. J. Cava, B. Batlogg, K. Kiyono, H. Takagi, J. J. Krajewski, W. F. Peck, L. W. Rupp, and C. H. Chen, Phys. Rev. B **49**, 11890 (1994).
[28] M. De Marco, D. Graf, J. Rijssenbeek, R. J. Cava, D. Z. Wang, Y. Tu, Z. F. Ren, J. H. Wang, M. Haka, S. Toorongian, M. Leone, and M. J. Naughton, Phys. Rev. B **60**, 7570 (1999).

[29] M. V. Rama Rao, V. G. Sathe, D. Sornadurai, B. Panigrahi, and T. Shripathi, J. Phys. Chem. Solids **61**, 1989 (2000).
[30] J. S. Lee, Y. Krockenberger, K. S. Takahashi, M. Kawasaki, and Y. Tokura, Phys. Rev. B **85**, 035101 (2012).
[31] K. Nakamoto, *Infrared and Raman Spectra of Inorganic and Coordination Compounds* (John Wiley & Sons, New York, 1986).
[32] G. Cao, J. Bolivar, S. McCall, J. E. Crow, and R. P. Guertin, Phys. Rev. B **57**, R11039 (1998).
[33] S. Sugai, H. Suzuki, Y. Takayanagi, T. Hosokawa, and N. Hayamizu, Phys. Rev. B **68**, 184504 (2003).
[34] E. Ya. Sherman, O. V. Misochko, and P. Lemmens, in *Spectroscopy of High-Tc Superconductors*, edited by N. M. Plakida (Taylor & Francis, London, 2003), pp. 97–158.
[35] P. D. C. King, T. Takayama, A. Tamai, E. Rozbicki, S. McKeown Walker, M. Shi, L. Patthey, R. G. Moore, D. Lu, K. M. Shen, H. Takagi, and F. Baumberger, Phys. Rev. B **87**, 241106(R) (2013).
[36] K.-Y. Choi, P. Lemmens, D. Heydhausen, G. Güntherodt, C. Baumann, R. Klingeler, P. Reutler, and B. Büchner, Phys. Rev. B **77**, 064415 (2008).
[37] See K.-Y. Choi, P. Lemmens, and H. Berger, Phys. Rev. B **83**, 174413 (2011), and references therein.
[38] L. Pintschovius, J. M. Bassat, P. Odier, F. Gervais, G. Chevrier, W. Reichardt, and F. Gompf, Phys. Rev. B **40**, 2229 (1989).
[39] A. I. Maksimov, O. V. Misochko, I. T. Tartakovsky, V. B. Timofeev, J. P. Remeika, A. S. Cooper, and Z. Fisk, Solid State Commun. **66**, 1077 (1988).